Subsurface hydrogen bonds at the polar Zn-terminated ZnO(0001) surface

Matti Hellström,[1] Igor Beinik,[2] Peter Broqvist,[1] Jeppe V. Lauritsen,[2] and Kersti Hermansson[1,*]
[1]*Department of Chemistry–Ångström, Uppsala University, Box 538, SE-75121 Uppsala, Sweden*
[2]*Interdisciplinary Nanoscience Center (iNANO), Aarhus University, Aarhus, Denmark*
(Received 19 August 2016; revised manuscript received 5 November 2016; published 27 December 2016)

The role of hydrogen and other defects in the stabilization of polar oxide interfaces is a matter of significant fundamental and practical interest. Using experimental (scanning tunneling microscopy, x-ray photoelectron spectroscopy) and theoretical (density functional theory) surface science techniques, we find that the polar Zn-terminated ZnO(0001) surface becomes excessively Zn deficient during high-temperature annealing (780 K) in ultrahigh vacuum (UHV). The Zn vacancies align themselves into rows parallel to the $[10\bar{1}0]$ direction, and the remaining surface Zn ions alternately occupy wurtzite (hcp) and zinc-blende (fcc) lattice positions, giving a characteristic "striped" $c(\sqrt{12}\times\sqrt{12})$R30° surface morphology with three types of rows: wurtzite Zn, zinc-blende Zn, and Zn vacancies. Interstitial H plays a central role in such a reconstruction, as it helps to compensate the excessive Zn deficiency. We propose a model in which hydrogen occupies positions in half of the vacancy rows to form hydroxide ions that can participate in hydrogen bonds in the O subsurface layer as a result of the mixed wurtzite/zinc-blende stacking.

DOI: 10.1103/PhysRevB.94.245433

I. INTRODUCTION

Zinc oxide (ZnO) is a wide-band-gap semiconductor that is used in a wide variety of applications: gas sensors, catalysts, and micro- and optoelectronic devices [1,2]. ZnO crystallizes in the hexagonal wurtzite structure (space group $P6_3mc$) at ambient conditions, and cleavage of the bulk structure perpendicular to the principal c crystal direction ([0001]) yields the two well-known polar Zn-terminated (0001) and O-terminated $(000\bar{1})$ surfaces [3]. These surfaces are so-called Tasker type-3 surfaces [4] that are intrinsically unstable unless there is some form of stabilization mechanism in play [5]. The nature of these stabilization mechanisms for the polar ZnO surfaces has been under intense investigation for a number of years [6–18] because of the fundamental importance of stabilization mechanisms for polar surfaces in materials science [5].

In some of the previous studies of polar ZnO surfaces, hydrogen was shown to play a role in the stabilization mechanism, most frequently in the form of OH groups. As-grown ZnO crystals normally contain substantial amounts of H impurities, which are likely to be the source of the zinc oxide n-type conductivity [19]. It is possible to "metallize" some ZnO surfaces through exposure to gas-phase H [20], but the influence that the "intrinsic" H impurities have on the electronic and geometric structures of ZnO surfaces is still not well understood. We show here that such H impurities can have a pronounced impact on the resulting ZnO surface morphology, even in ultrahigh vacuum (UHV).

In the present paper, we focus only on the Zn-terminated (0001) surface. In a gaseous environment, this surface can be stabilized by the adsorption of negative ions like O^{2-} [11] and OH^- [10,11,17], while under UHV conditions different kinds of surface reconstructions that give rise to Zn-deficient surface stoichiometries occur.

Scanning tunneling microscopy (STM) experiments have shown that the ZnO(0001) surface can be intrinsically stabilized by the formation of large triangular pits and islands with O-terminated step edges [7,8], hexagonal pits [13], a vicinal $(10\bar{1}4)$ surface facet at an angle of 22° to the (0001) surface [16], and adsorbed O^{2-} possibly coming from the O^{2-} atomic layer below the surface Zn^{2+} layer [18]. Also, an apparent $p(1\times3)$ reconstruction has been seen with noncontact atomic force microscopy (NC-AFM), where every *third* surface Zn^{2+} ion was interpreted as missing and the vacancies were aligned into an ordered pattern of rows (stripes) [12].

This last reconstruction is of particular interest since it is in apparent violation of the "electron counting rule" (ECR; sometimes called the "electron counting model") [21,22], which requires that there are no partially filled dangling bonds at the surface (and, consequently, that the surface is semiconducting). This occurs if the surface has a stoichiometry such that the net Zn deficiency corresponds to the removal of every *fourth* surface Zn^{2+} ion (the Zn deficiency $\theta\approx-0.25$ [23]); such a Zn-deficient stoichiometry is also the best on electrostatic grounds [23] and has been found to occur at the surface in experimental studies [13,16]. Indeed, theoretical studies employing empirical [24], semiempirical [25], or density functional methods [8,23,26,27] have also shown that a Zn deficiency $\theta\approx-0.25$ is particularly favorable, although other stoichiometries can be more stable depending on the chemical potential (partial pressure) of oxygen.

Here, we present a model based on STM and x-ray photoelectron spectroscopy (XPS) experiments and density functional theory (DFT) calculations, showing that the Zn-terminated (0001) surface can reconstruct into ordered rows of Zn vacancies in a $c(\sqrt{12}\times\sqrt{12})$R30° pattern; we believe this to be the same reconstruction that was reported as a $p(1\times3)$ reconstruction in Ref. [12]. Nevertheless, our interpretation of the atomic structure differs considerably from what was previously proposed. Our most important conclusions are that (i) the vacancy rows extend along a different crystal direction from what was previously thought, (ii) the ECR is not violated because H^+ from the bulk of the crystal is present at the surface and compensates the excessive Zn deficiency, (iii) the remaining rows of Zn ions alternately occupy wurtzite

*kersti@kemi.uu.se

and zinc-blende stacking positions [similar to how mixed wurtzite/zinc-blende hexagonal islands were shown to form at the O-terminated ZnO(000$\bar{1}$) surface] [14,15], and (iv) the wurtzite/zinc-blende stacking allows for the formation of hydrogen bonding in the O^{2-} sublayer.

The reconstruction is found to be metastable, meaning that there is at least one surface reconstruction, at the same Zn/O/H chemical potentials, which is thermodynamically more stable. Nevertheless, the present work illustrates the presence of several new phenomena, namely, the subsurface hydrogen bonding and mixed wurtzite/zinc-blende stacking, at the Zn-terminated ZnO(0001) surface.

II. METHOD

A. Experiments: STM and XPS

Hydrothermally grown ZnO(0001) single crystals were obtained from MTI Corp. The surface was cleaned by repeated cycles of Ar^+ ion sputtering (1 keV, 15 min) and annealing in UHV. STM, XPS, and temperature-programmed desorption (TPD) experiments were carried out in a UHV chamber with base pressure below 1.5×10^{-10} mbar at room temperature. Mass spectrometry performed in front of the crystal during annealing revealed that considerable amounts of O_2 and H_2 were emitted, and at high temperatures even some Zn was emitted, as reported in Ref. [28]. The overall pressure in the preparation chamber during the annealing cycles at 780 K did not exceed 8×10^{-10} mbar.

The O 1*s* x-ray photoelectron (XP) spectra were recorded using a laboratory Al Kα source with a photon energy of 1486.7 eV. The inelastic mean free path for the O 1s electrons was estimated to be 19.3 Å using the TPP-2M (Tanuma Powell and Penn algorithm) [29] predictive formula. Each O 1*s* peak was fitted with two Gaussian-Lorentzian line shapes after subtracting the Shirley background. The position of the second (smaller) component was constrained to be 1.4 eV separated from the main (lattice oxygen) peak. This higher-binding-energy component is commonly attributed in the literature to surface hydroxyl groups [17,28]. The effective OH coverage Θ_{OH} was estimated as

$$\Theta_{OH} = \frac{I_{OH}^{1s}/I_{O}^{1s}}{1 - \exp\left(\frac{-d}{\lambda_{ZnO}(KE)\cos(\phi)}\right)}, \quad (1)$$

where I_{OH}^{1s} and I_{O}^{1s} are the respective integral intensities, d is the ZnO interlayer distance, λ is the energy-dependent inelastic mean free path as estimated above, and ϕ is the emission angle relative to the sample normal.

B. DFT calculations

DFT calculations were here performed using the optB86b-vdW functional [30], which is designed to selfconsistently account for non-local correlation contributions, implemented in the VASP program [31–34], with core-valence interactions described by projector augmented-wave (PAW) potentials [35,36]. We also performed calculations using the Perdew-Burke-Ernzerhof (PBE) [37] and vdW-DF-cx [38] functionals and obtained results qualitatively similar to those for optB86b-vdW (see the Supplemental Material [39]). The ZnO(0001) surface was modeled as a six-double-layer-thick slab with the bottom (O-terminated) layer passivated by pseudoatoms of valency 0.5. The pseudoatoms and the atoms in the bottom two double layers were kept fixed in the geometry optimizations. The slabs were constructed from the optB86-vdW-optimized wurtzite ZnO lattice parameters $a = 3.258$ Å and $c = 5.265$ Å (in good agreement with room-temperature experimental values of $a = 3.250$ Å and $c = 5.207$ Å) [40].

The Brillouin zone was sampled using a Γ-centered k-point grid, the size of which depended on the size of the supercell: a $4 \times 4 \times 1$ grid (with the third direction being normal to the surface) was used for the 3×3 supercell, a $3 \times 3 \times 1$ grid was used for the 4×4 supercell, as well as for the orthorhombic supercell used for the calculation of the reconstructions containing H, and only the Γ point was used for the 6×6 supercell. The different supercells that were used in the calculations are shown in the SM. Simulated AFM images were obtained from the second derivative of the calculated electrostatic potential in the region 6.75–7.25 Å above the surface, using the method proposed by Chan *et al.* [41] (this method neglects any dynamics of both the tip and the surface). The vacuum gap (along z) was 20 Å, and a dipole correction was applied.

The stoichiometry of ZnO polar surface reconstructions (without H) can be characterized by means of the "Zn deficiency" θ:

$$\theta = -\frac{N_{\text{surface Zn vacancies}}}{N_{\text{surface Zn vacancies}} + N_{\text{remaining surface Zn atoms}}}. \quad (2)$$

Because different reconstructions have different stoichiometries, their relative stabilities are calculated in an *ab initio*-thermodynamics formalism [42] as a function of the chemical potential of oxygen μ_O:

$$E_s = \frac{1}{A}[E - n_{Zn}E(ZnO) - (n_O - n_{Zn})\mu_O] - \frac{1}{A}\left[E_{clean} - n_{Zn}^{clean}E(ZnO)\right], \quad (3)$$

where E_s is the surface formation energy per surface unit cell, A is the number of surface unit cells of the structure, E is the total energy, n_i is the number of atoms of element i, E(ZnO) is the total energy per formula unit of bulk wurtzite ZnO, and n_{Zn}^{clean} is the number of Zn atoms for a "clean" (bulk-truncated) reference surface with the same area as for the system with Zn vacancies. The lower limit for μ_O is when it would be favorable to form Zn metal, i.e., $E(ZnO) < \mu_O + E(Zn_{metal})$, and the upper limit is the energy per O in the O_2 molecule: $\mu_O < \frac{1}{2}E(O_2)$. It is customary to use the chemical potential relative to half the binding energy in the O_2 molecule, i.e.,

$$\Delta\mu_O = \mu_O - \tfrac{1}{2}E(O_2), \quad (4)$$

so that $\Delta\mu_O = 0.0$ eV in O-rich conditions. The chemical potential of oxygen can be related to different temperatures and pressures of O_2:

$$\Delta\mu_O(T,p) = \Delta\mu_O(T,p^\circ) + \frac{1}{2}\,kT\ln\left(\frac{p}{p^\circ}\right). \quad (5)$$

Thus, if the temperature dependence of μ_O for the pressure p° is known, any value of μ_O can be related to different T and p.

The enthalpy and entropy of O_2 are listed in thermochemical tables for different temperatures at the pressure $p^\circ = 1$ atm [43], and

$$\Delta\mu_O(T,p^\circ) = \tfrac{1}{2}[H(T,p^\circ,O_2) - H(0\ \mathrm{K},p^\circ,O_2)] - \tfrac{1}{2}T[S(T,p^\circ,O_2) - S(0\ \mathrm{K},p^\circ,O_2)]. \quad (6)$$

The relation between $\Delta\mu_O$ and different temperatures and pressures is given in the SM. See Ref. [42] for more details.

III. RESULTS AND DISCUSSION

Figure 1 shows the effect of the annealing temperature on the surface morphology. For low annealing temperatures [740 K, Fig. 1(a)] many triangular pits and islands of various sizes (1–3 nm) form, while for higher annealing temperatures (2–5 min at 780 K and slow cooldown of 15–20 min) large areas of the sample adopt a *striped* pattern, or periodic arrays of ordered rows [Figs. 1(b) and 1(c)]. The STM image in Fig. 1(b) also shows a triangular island near the right-hand side; notably, the rows form an angle of approximately 90° to the top edge of the triangle, which is $\{10\bar{1}0\}$ terminated. The spacings between the rows in Figs. 1(b) and 1(c) were determined from fast Fourier transforms of (40×40) nm^2 STM images to be 0.9 ± 0.1 nm. The stripes appear somewhat "wavy," either due to thermal drift during STM imaging or due to some intrinsic disorder in the surface Zn vacancy structure. A prolonged high-temperature annealing, which could potentially lead to a better ordering, resulted in a significant deterioration of the sample conductivity, which rendered further STM measurements impossible.

The lack of atomic resolution in the STM measurements makes it difficult to draw any immediate conclusions about the exact structure of the surface. However, the appearance and the periodicity of the stripes are very similar to those previously reported by Torbrügge *et al.* [12], who also obtained stripes when annealing the ZnO(0001) surface at high temperatures (1150 K in their case). They obtained near-atomic resolution in their NC-AFM experiments and reported that the distance between the rows was 0.98 nm, which corresponds to three lattice spacings along the a direction ($3 \times 0.325 = 0.975$ nm). We reproduce one of their NC-AFM images in Fig. 1(d), which is an averaged image over a large area of the surface. There are two features which will be of particular importance in the following discussion: (i) There seem to be three distinctly different types of rows (dark, "medium," and bright), and (ii) these rows are periodically repeated; in particular, the bright rows are always diagonally down and to the left of the dark rows in the NC-AFM image.

The surface structure for the stripes proposed by Torbrügge *et al.* [12] is shown in Fig. 2(a). Every third surface Zn row is missing, and the rows of surface vacancies are parallel to $[1\bar{2}10]$ (the horizontal direction in the top views in Fig. 2). There was, however, a slight mismatch between the expected spacing of the vacancy rows in such a model ($3a \sin 60^\circ = 0.844$ nm) and the actually measured spacing ($3a = 0.975$ nm) that could have originated from thermal drift [12]. Nevertheless, a consideration of possible surface structures as judged from our DFT calculations and STM data (as well as previously reported NC-AFM data) suggested to us that the vacancy rows do not, in fact, run parallel to $[1\bar{2}10]$ but are rotated 90° (or, equivalently, 30°) and thus run parallel to $[10\bar{1}0]$ instead [see Fig. 2(b); the vacancy rows are labeled "1"].

Evidence that rows of vacancies preferentially align along $[10\bar{1}0]$ and not $[1\bar{2}10]$ is obtained from DFT calculations performed for Zn deficiencies $\theta = -1/6$, $-1/4$, and $-1/3$ where the surface Zn vacancies were aligned into rows. Figure 2(c) shows that, for all Zn deficiencies, aligning the rows along $[10\bar{1}0]$ (solid lines) is at least 0.04 eV per (1×1) surface unit cell more stable than aligning them along $[1\bar{2}10]$ (dashed lines). These results can intuitively be understood since the vacancies are (effectively) negatively charged and aligning the vacancies along $[1\bar{2}10]$ causes them to be "nearest neighbors" (the shortest intervacancy distance then being $a = 0.325$ nm), while aligning them along $[10\bar{1}0]$ gives longer intervacancy distances (the shortest intervacancy distance being $\sqrt{3}a = 0.563$ nm).

Figure 2(b) illustrates how vacancy rows separated by 0.975 nm make up every *sixth* row parallel to $[10\bar{1}0]$, and this reconstruction thus fails to obey the ECR. In between the vacancy rows there are five rows of surface Zn ions (rows

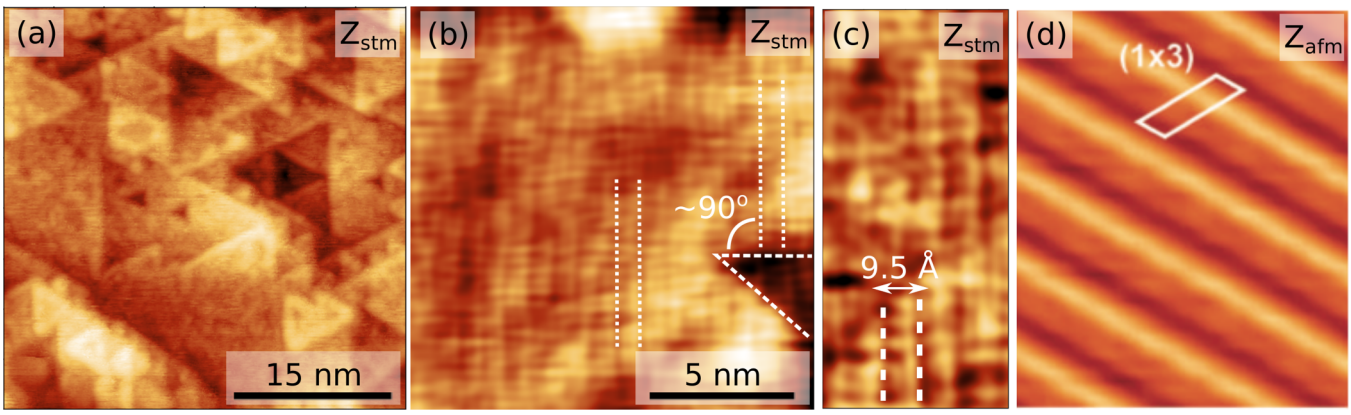

FIG. 1. Surface morphologies of the ZnO(0001) surface. (a) STM image of triangular pits and islands (sample annealed at 740 K). (b)–(c) STM images of the striped reconstruction (sample annealed at 780 K) recorded in constant-current mode at ~ 2 V of sample bias. (d) An NC-AFM image averaged over a (6×6) nm^2 area of the surface; reprinted (adapted) with permission from J. Phys. Chem. C **133**, 4909 (2009). Copyright 2009 American Chemical Society.

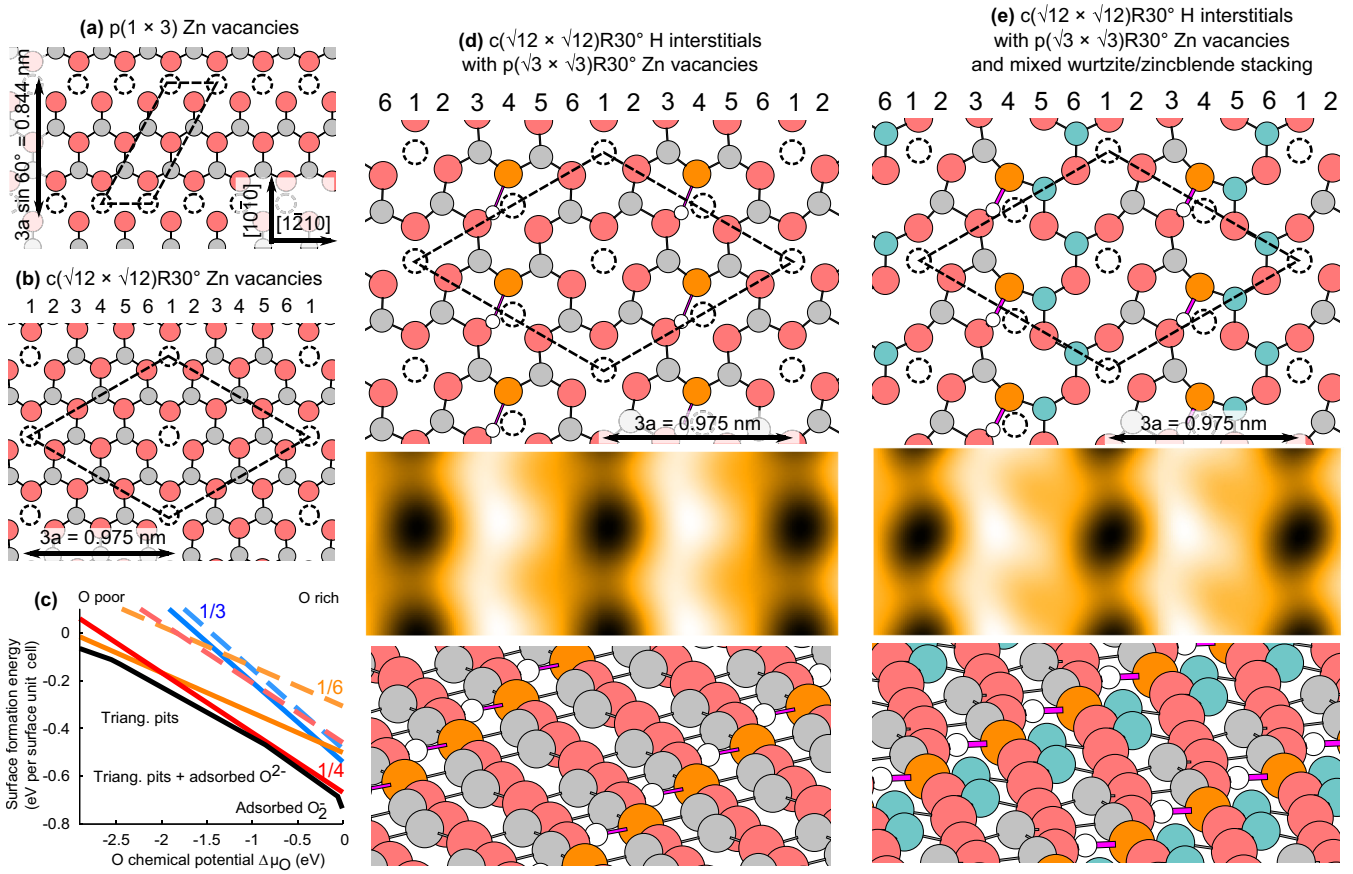

FIG. 2. Top views of surface reconstructions (only the atoms in the surface double layer are shown; Zn is gray, O is red, and Zn vacancies are indicated by dashed circles): (a) $p(1 \times 3)$ surface Zn vacancies (proposed atomic structure of the reconstruction in Ref. [12]); the vacancy rows run parallel to $[1\bar{2}10]$, $\theta = -1/3$. (b) $c(\sqrt{12} \times \sqrt{12})$R30° surface Zn vacancies; the vacancy rows run parallel to $[10\bar{1}0]$, $\theta = -1/6$. (c) Calculated surface formation energies of stripes along $[1\bar{2}10]$ (dashed lines) and along $[10\bar{1}0]$ (solid lines) for different Zn deficiencies. Also shown are the most stable reconstructions from previous works (black; see also the Supplemental Material) [23,26]. (d) From top to bottom: top view of a reconstruction including H, with the hydrogen-bond-accepting O ions colored orange and hydrogen bonds drawn in pink, simulated AFM, and perspective view. (e) Reconstruction similar to that in (d), but half of the Zn ions (in rows 5–6) occupy zinc-blende positions (colored blue).

2–6). In the NC-AFM experiments by Torbrügge *et al.* [12] there appeared to be groups of two parallel rows of Zn ions separated by the vacancy rows. If the row in the middle between the vacancy rows (row 4) in Fig. 2(b) is replaced by vacancies, the resulting $p(\sqrt{3} \times \sqrt{3})$R30° pattern has a Zn deficiency $\theta = -1/3$ and also fails to obey the ECR.

In fact, because the smallest repeating unit contains six primitive surface unit cells, no amount of surface vacancies could give rise to a surface Zn deficiency of $-1/4$. However, if the middle row (row 4) is replaced by a monovalent impurity (e.g., a group-I element like H or Li), in electrostatic terms this effectively corresponds to removing only one half of a Zn^{2+} ion. Together with the actual Zn vacancy the effective Zn deficiency would be $\theta_{\text{eff}} = -1\frac{1}{2}/6 = -1/4$, and thus, the ECR is obeyed. Both H and Li are known to occur in substantial amounts in hydrothermally grown ZnO, which makes their presence at the surface plausible.

The chemical composition at the surface was elucidated by means of XPS measurements, which revealed that substantial amounts of H (in form of OH groups) were present at the surface, whereas no evidence of Li could be seen. The XPS measurements in Fig. 3 show that the effective coverage estimated for the freshly introduced sample cleaned by three cycles of sputtering at 1 kV followed by UHV annealing at 730 K [Fig. 3(a)] was $\Theta_{\text{OH}} \approx 3.2$ monolayers (ML; for $d = 2.7$ Å, $\lambda = 19.3$ Å, and $\phi = 0$) and clearly exceeded the amount that the surface could accommodate. Therefore, we conclude that some amount of hydroxyls is hidden in the subsurface region. For the sample annealed at 770 K [Fig. 3(b)], $\Theta_{\text{OH}} \approx 0.8$ ML. Taking into account a rather large probing depth in our experiments, we cannot exclude the possibility that a large fraction of these hydroxyls also settles in the subsurface region. The effective OH coverage slowly decreases with the number of sputter-anneal cycles; however, we never observed that the OH component would vanish away completely.

Moreover, in TPD measurements, substantial amounts of H_2 (and only minute amounts of Li) were found to be emitted from the crystal upon annealing [28], which shows that H at some point has "passed" the surface during preparation.

Both XPS and TPD thus support the notion that H is present at the surface. Torbrügge *et al.* [12] also proposed that H could be present in the surface region, and previous DFT calculations

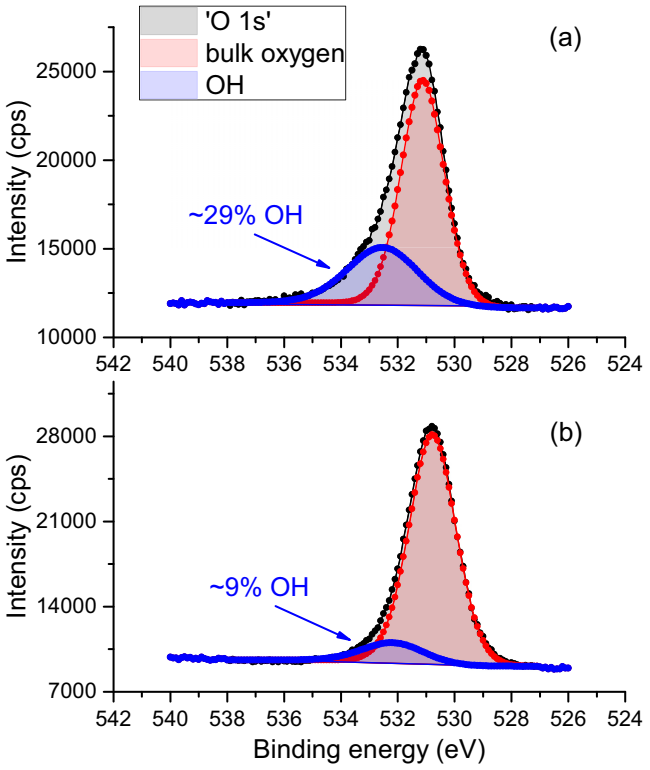

FIG. 3. (a) A characteristic XP spectrum recorded from an as-received ZnO(0001) surface after three cycles of Ar^+ sputtering at 1 kV for 20 min followed by annealing at 730 K in UHV. (b) A characteristic XP spectrum recorded from the same sample after an additional eight cycles of sputtering with the same parameters followed by UHV annealing at 770 K.

have shown that the presence of surface H at ZnO(0001) could affect the surface morphology [44]. Recently, H was found to stabilize the presence of Zn vacancies also at the O-terminated $(000\bar{1})$ surface [45]. Subsurface H has also previously been found in, for example, rutile TiO_2 [46].

The structural model in Fig. 2(b) has the correct spacing between the vacancy rows but a surface stoichiometry that does not obey the ECR. However, if the Zn atoms in row 4 are replaced by H atoms, the H atoms can displace towards one of the neighboring O ions either along the direction of the row ($[10\bar{1}0]$, row 4) or in neighboring rows [row 3 or row 5, Fig. 2(d)]. Our DFT calculations suggest that both possibilities are equally stable (within 0.005 eV per H atom). When the H atom attaches to an O ion in row 3 (or row 5), a hydrogen bond is formed to the nearest row-4 O, i.e., O(row 3)–H $\cdots$ O(row 4) [the O ions in row 4 are colored orange in Fig. 2(d) to indicate this; the hydrogen bonds are drawn as pink lines]. The H atoms do not "stick out" from the surface but lie more or less in the plane of the O sublayer, as seen in the perspective view in Fig. 2(d). The surface layer Zn ions also relax towards the underlying O ions (in the bulk the Zn and O layers are 0.6 Å apart but at the surface only ~0.3 Å).

In the NC-AFM image by Torbrügge *et al.* [12] [Fig. 1(d)], there were three types of visible rows: dark, medium, and bright. Similarly, in our STM images [Figs. 1(b) and 1(c)], the contrast between the rows of ions and the rows of vacancies is often more pronounced on the left-hand side of the vacancy rows. Although the simulated AFM image in Fig. 2(d) reproduces the most prominent features of the experimental AFM image in Fig. 1(d) (the three different types of rows), there is no particular reason why the H should consistently favor the "left" side of the vacancy since the left and right sides are symmetry equivalent. Indeed, our calculations suggest that a structure with the H alternating between the left and right sides of a row is as stable (within 0.004 eV per H) as the one depicted in Fig. 2(d).

If, however, the Zn ions in rows 5–6 from Fig. 2(d) are displaced along $[10\bar{1}0]$ so that they occupy fcc (zinc-blende) instead of hcp (wurtzite) positions [see Fig. 2(e)], this gives two fundamentally different rows of Zn ions, and the configuration in Fig. 2(e) is 0.03 eV per H more stable than that in Fig. 2(d). Although the calculations suggest that the wurtzite/zinc-blende stacking is favored, the energy difference from the wurtzite/wurtzite stacking is small, and coexistence of the two stacking patterns could therefore exist on the surface, which might be a possible reason for the rather wavy stripes in Fig. 1(b). It is not very surprising to find that shifting (some of) the surface ions to zinc-blende positions is favorable: at the O-terminated $(000\bar{1})$ surface, such reconstructions have been shown to occur with alternating hexagonal islands of wurtzite/zinc-blende stacking [14,15]. On ZnO(0001), the alternating wurtzite and zinc-blende stacking instead occurs in the form of rows.

There are two reasons the mixed wurtzite/zinc-blende stacking is favorable. The first is that the positive Zn ions in row 6 come closer to the negative vacancies in row 1. The second involves hydrogen bonding in the O subsurface layer: In the wurtzite/wurtzite stacking [Fig. 2(d)] structure, the hydrogen bond is very long (2.17 Å) and consequently weak. It is unfavorable for the O in row 4 to move closer to the H since the O is "trapped" by the neighboring Zn ions in rows 3 and 5. As a consequence, the O–H $\cdots$ O angle in the lateral plane becomes 143°, which is quite far from the ideal value of 180°. However, when the Zn ions in row 5 are moved "down" to zinc-blende positions [Fig. 2(e)], this allows for O(row 4) to move much closer to the hydrogen (hydrogen bond length of 1.87 Å), giving a much stronger hydrogen bond. The O–H $\cdots$ O angle also increases to 154°.

The configuration in Fig. 2(e) is the most stable that we have found where stripes are formed along $[10\bar{1}0]$ (adsorbing the H on row 2/row 3 is 0.02 eV per H more stable than adsorbing on rows 1, 4, or 5/6). However, it is considerably less stable than many other kinds of reconstructions; for example, Valtiner *et al.* [11] proposed that the ZnO(0001) surface could be stabilized by a mixed O^{2-}/OH^- adsorption pattern when exposed to humid oxygen. That reconstruction nominally has the same surface stoichiometry (Zn deficiency and H concentration) as ours and is thermodynamically much more stable [by 0.08 eV per (1×1) surface unit cell, or 0.48 eV per H atom, according to our calculations]. Nevertheless, the striped reconstruction [Fig. 2(e)] can form at very high annealing temperatures since this leads to the desorption of any adsorbed O^{2-}, OH^-, and even a small amount of Zn^{2+} (as seen in our TPD measurements). When the Zn^{2+} desorbs, highly mobile H from the bulk can diffuse to the surface and compensate the

excessive Zn deficiency. Under these conditions, the striped phase in Fig. 2(e) forms, but it is most likely metastable; that is, the system is not in thermodynamic equilibrium.

A plethora of possible surface reconstructions has been presented for the polar Zn-terminated ZnO(0001) surface in the literature [7,8,10–13,16–18]. Thus, it seems likely that the prevailing stabilization mechanism for any given crystal could possibly depend on the history of the crystal, for example, with respect to how it was synthesized or the extent of any previous annealing cycles performed. Such procedures would likely influence the number and types of defects in the crystal (for example, with respect to H impurities that are crucial for the reconstruction seen in the present paper). Moreover, the formation of a particular reconstruction might also be sensitive to any residual hydrogen or water in the atmosphere surrounding the crystal.

IV. CONCLUSIONS

We have shown that the annealing of a hydrothermally grown ZnO(0001) single crystal in UHV leads to large, flat morphologies characterized by periodic arrays of rows (stripes). Every third Zn ion is missing from the surface, but the excessive Zn deficiency is compensated by interstitial H. It is favorable for every second row of surface Zn ions to displace from their wurtzite stacking positions into zinc-blende stacking positions, which allows for the formation of hydrogen bonds in the O atomic layer beneath the surface. These results illustrate the significant impact that H impurities have on the structure of the polar ZnO(0001)-Zn surface upon annealing in ultrahigh vacuum.

ACKNOWLEDGMENTS

We acknowledge useful discussions with S. E. Huber, J. Kullgren, and M. J. Wolf. This work was performed within the framework of the EU COST Action CM1104 (Reducible oxide chemistry, structure, and functions) and was supported by Lennanders stipendiestiftelse, the Swedish Research Council (VR), the Swedish national strategic e-science research program eSSENCE, ERC Starting Grant No. 239834, and Haldor Topsøe A/S. Computational resources were provided by SNIC at NSC.

[1] C. F. Klingshirn, B. K. Meyer, A. Waag, A. Hoffmann, and J. Geurts, *Zinc Oxide: From Fundamental Properties Towards Novel Applications* (Springer, Berlin, 2010).
[2] R. M. Hewlett and M. A. McLachlan, Adv. Mater. **28**, 3893 (2016).
[3] C. Wöll, Prog. Surf. Sci. **82**, 55 (2007).
[4] P. W. Tasker, J. Phys. C **12**, 4977 (1979).
[5] J. Goniakowski, F. Finocchi, and C. Noguera, Rep. Prog. Phys. **71**, 016501 (2008).
[6] M. Kunat, S. Gil Girol, T. Becker, U. Burghaus, and C. Wöll, Phys. Rev. B **66**, 081402 (2002).
[7] O. Dulub, L. A. Boatner, and U. Diebold, Surf. Sci. **504**, 271 (2002).
[8] O. Dulub, U. Diebold, and G. Kresse, Phys. Rev. Lett. **90**, 016102 (2003).
[9] B. Meyer, Phys. Rev. B **69**, 045416 (2004).
[10] M. Valtiner, S. Borodin, and G. Grundmeier, Phys. Chem. Chem. Phys. **9**, 2406 (2007).
[11] M. Valtiner, M. Todorova, G. Grundmeier, and J. Neugebauer, Phys. Rev. Lett. **103**, 065502 (2009).
[12] S. Torbrügge, F. Ostendorf, and M. Reichling, J. Phys. Chem. C **113**, 4909 (2009).
[13] J. H. Lai, S. H. Su, H.-H. Chen, J. C. A. Huang, and C.-L. Wu, Phys. Rev. B **82**, 155406 (2010).
[14] J. V. Lauritsen, S. Porsgaard, M. K. Rasmussen, M. C. R. Jensen, R. Bechstein, K. Meinander, B. S. Clausen, S. Helveg, R. Wahl, G. Kresse *et al.*, ACS Nano **5**, 5987 (2011).
[15] R. Wahl, J. V. Lauritsen, F. Besenbacher, and G. Kresse, Phys. Rev. B **87**, 085313 (2013).
[16] H. Zheng, M. Gruyters, E. Pehlke, and R. Berndt, Phys. Rev. Lett. **111**, 086101 (2013).
[17] R. Heinhold, G. T. Williams, S. P. Cooil, D. A. Evans, and M. W. Allen, Phys. Rev. B **88**, 235315 (2013).
[18] H. Xu, L. Dong, X. Q. Shi, M. A. Van Hove, W. K. Ho, N. Lin, H. S. Wu, and S. Y. Tong, Phys. Rev. B **89**, 235403 (2014).
[19] A. Janotti and C. G. Van de Walle, Nat. Mater. **6**, 44 (2007).
[20] Y. Wang, B. Meyer, X. Yin, M. Kunat, D. Langenberg, F. Traeger, A. Birkner, and C. Wöll, Phys. Rev. Lett. **95**, 266104 (2005).
[21] M. D. Pashley, Phys. Rev. B **40**, 10481 (1989).
[22] M.-H. Du, S. B. Zhang, J. E. Northrup, and S. C. Erwin, Phys. Rev. B **78**, 155424 (2008).
[23] G. Kresse, O. Dulub, and U. Diebold, Phys. Rev. B **68**, 245409 (2003).
[24] H. Meskine and P. A. Mulheran, Phys. Rev. B **84**, 165430 (2011).
[25] S. E. Huber, M. Hellström, M. Probst, K. Hermansson, and P. Broqvist, Surf. Sci. **628**, 50 (2014).
[26] O. Warschkow, K. Chuasiripattana, M. J. Lyle, B. Delley, and C. Stampfl, Phys. Rev. B **84**, 125311 (2011).
[27] S. Pal, T. Jasper-Tönnies, M. Hack, and E. Pehlke, Phys. Rev. B **87**, 085445 (2013).
[28] I. Beinik, M. Hellström, T. N. Jensen, P. Broqvist, and J. V. Lauritsen, Nat. Commun. **6**, 8845 (2015).
[29] S. Tanuma, C. J. Powell, and D. R. Penn, Surf. Interf. Anal. **21**, 165 (1994).
[30] J. Klimeš, D. R. Bowler, and A. Michaelides, Phys. Rev. B **83**, 195131 (2011).
[31] G. Kresse and J. Hafner, Phys. Rev. B **47**, 558 (1993).
[32] G. Kresse and J. Furthmüller, Comput. Mater. Sci. **6**, 15 (1996).
[33] G. Kresse and J. Furthmüller, Phys. Rev. B **54**, 11169 (1996).
[34] G. Kresse and J. Hafner, Phys. Rev. B **49**, 14251 (1994).
[35] P. E. Blöchl, Phys. Rev. B **50**, 17953 (1994).
[36] G. Kresse and D. Joubert, Phys. Rev. B **59**, 1758 (1999).
[37] J. P. Perdew, K. Burke, and M. Ernzerhof, Phys. Rev. Lett. **77**, 3865 (1996).
[38] K. Berland and P. Hyldgaard, Phys. Rev. B **89**, 035412 (2014).
[39] See Supplemental Material at http://link.aps.org/supplemental/10.1103/PhysRevB.94.245433 for the structures of the reconstructions in Fig. 2(c), as well as results calculated with different density functionals.

[40] J. Albertsson, S. C. Abrahams, and Å. Kvick, Acta Crystallogr., Sect. B **45**, 34 (1989).
[41] T.-L. Chan, C. Z. Wang, K. M. Ho, and J. R. Chelikowsky, Phys. Rev. Lett. **102**, 176101 (2009).
[42] K. Reuter and M. Scheffler, Phys. Rev. B **65**, 035406 (2001).
[43] M. W. Chase, Jr., J. Phys. Chem. Ref. Data **Monograph 9**, 1 (1998).
[44] M. Valtiner, M. Todorova, and J. Neugebauer, Phys. Rev. B **82**, 165418 (2010).
[45] R. Jacobs, B. Zheng, B. Puchala, P. M. Voyles, A. B. Yankovich, and D. Morgan, J. Phys. Chem. Lett. **7**, 4483 (2016).
[46] G. H. Enevoldsen, H. P. Pinto, A. S. Foster, M. C. R. Jensen, W. A. Hofer, B. Hammer, J. V. Lauritsen, and F. Besenbacher, Phys. Rev. Lett. **102**, 136103 (2009).